Asian Journal of Chemistry; Vol. 37, No. 12 (2025), 3211-3218
ASIAN JOURNAL OF CHEMISTRY
https://doi.org/10.14233/ajchem.2025.35000

Comparative Studies of Chemically and Green Synthesized $CoFe_2O_4$, $Ni_{0.5}Co_{0.5}Fe_2O_4$, $Li_{0.5}Co_{0.75}Fe_2O_4$ Nanoparticles *via* Sol-Gel Method for Electrical and Antibacterial Applications

G. GOWRI SHANMUGAPRIYA[1,2], C. YOGAMBAL[3], S. UMAMAHESWARI[1], R. RAJIKHA[1], S. ANALISA[1], C. SUBRAMANIYAN[4] and V. SATHANA[1,*]

[1]Department of Physics, St. Joseph's College of Arts and Science (Autonomous), Cuddalore-607001, India
[2]Department of Physics, V.R.S. College of Engineering and Technology, Arasur, Villupuram-607107, India
[3]Department of Physics, IFET College of Engineering (Autonomous), Villupuram-605108, India
[4]Department of Mechanical Engineering, V.R.S. College of Engineering and Technology, Arasur, Villupuram-607107, India

*Corresponding author: E-mail: sathana@sjctnc.edu.in

Received: 3 October 2025 *Accepted*: 27 November 2025 *Published online*: 30 November 2025 AJC-22213

This study investigates the electrical and antibacterial properties of cobalt ferrite ($CoFe_2O_4$) nickel-doped cobalt ferrite ($Ni_xCo_{1-x}Fe_2O_4$) and lithium-doped cobalt ferrite ($Li_xCo_{1-x/2}Fe_2O_4$) where x = 0.5 synthesized *via* sol-gel technique using *Allium sativum* extract (green route) and citric acid (chemical route). The synthesized nanoparticles were characterized by XRD, SEM, EDS and FTIR to analyze their structural and morphological properties. The XRD analysis confirmed that $Ni_{0.5}Co_{0.5}Fe_2O_4$, $Li_{0.5}Co_{0.75}Fe_2O_4$ and $CoFe_2O_4$ compounds are well-crystallized and adopt a cubic spinel structure. The SEM images show distinct morphological changes between the variation of materials synthesis namely, chemically synthesized nanoparticles exhibit well-structured cubic phase, whereas green-synthesized nanoparticles display encapsulated and some irregular morphologies, probably due to the capping effect of the bioactive compound *A. sativum* extract used as chelating agent. The study on EDS confirmed the presence of all expected constituent elements in their stoichiometric ratios, verifying the successful synthesis of ferrite nanoparticles in the pure form. The analysis of synthesized samples through impedance spectroscopy confirmed that the green synthesis has lower bulk resistance and enhanced electrical conductivity comparative to chemically synthesized compounds. Among all compositions, Ni-doped cobalt ferrite (sol-gel route) exhibited the highest electrical conductivity, while green-synthesized $Li_{0.5}Co_{0.75}Fe_2O_4$ showed promising electrochemical behaviour, indicating its potential as an efficient anode material for lithium-ion batteries. Moreover, the antibacterial examines against both Gram-positive and Gram-negative bacterial strains confirmed that the green-synthesized nanoparticles demonstrate a significant and greater antimicrobial activity across all compounds. Therefore, this study highlights the benefits of plant-mediated green synthesis as a sustainable and effective alternative to conventional sol-gel techniques for fabricating multifunctional ferrite nanomaterials with improved electrical and antibacterial routine.

Keywords: *Allium sativum*, Sol-gel synthesis, Cobalt ferrites, Antibacterial activity, Electrical properties.

INTRODUCTION

Nanotechnology has opened a new way for development in many fields, including materials science, biomedicine and electronics. It plays an important role in enhancing products such as therapeutics, biosensors, sunscreens and drug delivery systems [1-4]. The materials used in this study consist of lithium, a lightweight alkali metal with industrial significance but potential toxicity in high doses; nickel, known for its corrosion resistance, mainly when alloyed with chromium and copper, garlic (*Allium sativum*), widely used vegetable rich in phenolic compounds with antioxidant, antibacterial and cardiovascular benefits. It is widely used for cooking, also for traditional herbal medicines. Garlic contains bioactive sulphur compounds, including allicin and S-allyl cysteine, which impart strong antioxidant and antibacterial properties. The active compound allicin contributes to its distinctive flavour and bioactivity [5-7]. Instead of conventional chemical synthesis, green synthesis method such as sol-gel method is eco-friendly and cost-effective. Many advantages like time consumption for processing, high purity reduction of contamination, porosity and particle size by transforming sol to gel has been achieved.

Sol-gel process is a simple, cost effective and efficient among various methods, of preparation of nanomaterials especially pure and well-structured ferrite nanomaterials. The primary objectives of this research include synthesizing nickel

and lithium-doped cobalt ferrite nanoparticles using both chemical and green sol-gel methods, investigating the impact of *A. sativum* extract on thsse structural and morphological properties of the synthesized nanoparticles, comparing the electrical, magnetic and antibacterial properties of chemically synthesized and green-synthesized nanoparticles and evaluating the potential of green-synthesized ferrites for biomedical and electronic applications. The unique characteristics of ferrite materials made useful for distinct application domains both electrochemical and antibacterial applications [8-10]. Moreover, tunable cation distribution and defect structures in synthesized Co, Ni and Li ferrites govern their charge transport and surface redox behaviour, enabling their dual function as efficient energy-storage electrodes and potent antibacterial agents through semiconducting activity and metal-ion release [11,12]. These characteristics enhance the efficacy of antibacterial activity and oxygen species formation. Hence, assessing both properties in a combined study delivers a whole structure-function relation of these ferrites in various applications. The use of *A. sativum* extract in the synthesis of ferrite nanoparticles not only reduces the hazard and also increases the biocompatibility and functionality of the nanoparticles. The electrochemical performance reflects charge transfer efficiency and electronic conduction, the antibacterial effectiveness depends on surface bacteria interactions and reactive oxygen species formation. The method of preparation and changes in structure strongly influence the multifunctional properties of the compounds.

EXPERIMENTAL

The precursor materials used in the synthesis process were lithium nitrate [$LiNO_3$], cobalt nitrate [$Co(NO_3)_2{\cdot}6H_2O$], nickel nitrate [$Ni(NO_3)_2{\cdot}6H_2O$], ferric nitrate [$Fe(NO_3)_3{\cdot}9H_2O$] and citric acid [$C_6H_8O_7{\cdot}H_2O$] and were procured from Sigma-Aldrich, USA. Distilled water was used to prepare all the necessary solutions. *Allium sativum* (garlic) was purchased from the local vegetable shop.

Preparation of cobalt ferrite, nickel- and lithium-doped cobalt ferrite nanoparticles (chemical method): Cobalt ferrite ($CoFe_2O_4$), nickel- and lithium-doped cobalt ferrite nanoparticles [$Ni_{0.5}Co_{0.5}Fe_2O_4$ and $Li_{0.5}Co_{0.75}Fe_2O_4$] were synthesized using the sol-gel technique. A homogenous solution was obtained by dissolving the required metal nitrates in deionized water and then citric acid was added as a chelating agent to mix the metal ions uniformly. The pH of the solution was adjusted to approximately 7 using an ammonia solution to stabilize the mixture. The mixture was then continuously stirred at 80 ºC for 6 h, provides the formation of a viscous gel. This gel was then subjected to combustion at 250 ºC to produce a fine powder. The developed powder was then annealed at 800 ºC for 6 h to improve crystallinity and confirm purity of the prepared ferrite nanomaterials.

Green method: In an eco-friendly approach, *A. sativum* (garlic) extract [13,14] was employed as reducing and capping agent for the green synthesis of ferrite nanoparticles. Fresh garlic cloves were crushed and the filtrate was used within 24 h to preserve its bioactive components. The filtered extract was now mixed with the mixture of precursors in aqueous media. Phytochemicals present in *A. sativum* such as allicin and flavonoids being strong complexing and reducing agents, react rapidly in the mixture, promoting a uniform gelation process and controlled nucleation before decomposition at 100 ºC. To obtain a uniform gel, the mixture was adjusted to pH 7 with ammonia and stirred at 80 ºC for 6 h consistently. The obtained gel was preheated at 250 ºC to obtain a fine, fluffy powder, followed by gentle grinding to achieve well-dispersed compound.

Characterization: X-ray diffraction (model: Rigaku Miniflex II X-ray diffractometer) was employed to confirm phase purity, determine crystallite size and analyse lattice parameters. Fourier transform infrared spectroscopy (model: Perkin-Elmer Spectrum Two FTIR spectrometer) was used to identify functional groups and verify the presence of capping agents in green-synthesized nanoparticles. Scanning electron microscopy (model: FEI Quanta 250 FEG SEM) was used for finding the surface morphology and particle size distribution. The elemental composition and stoichiometry of the synthesized ferrites were confirmed by energy dispersive X-ray spectroscopy (EDAX) attached to SEM. To investigate the electrical properties of the synthesized ferrites, AC impedance spectroscopy was performed on the pelletized samples using a Wayne Kerr 6500B Impedance Analyzer. The pellets were prepared with a hydraulic laboratory pellet press under 6 GPa uniaxial pressure. The pellets had a thickness of 3 mm and a diameter of 10 mm and both surfaces were coated with silver paste to ensure proper electrode contact. The samples were dried at 200 ºC for 1 h before measurement. Electrical properties were also measured with the same instrument, over a frequency range of 20 Hz to 15 MHz.

Antibacterial studies: In this work, the agar diffusion method was used to evaluate the antibacterial activity of the prepared spinal ferrites. In this procedure, bacterial cultures are evenly spread onto nutrient agar Petri dishes to form a uniform lawn. Sterile forceps were used to place antibiotic discs or nanoparticles onto the agar surface. The plates were incubated at 37 ºC for 24 h to allow the bacterial growth. Following incubation, the diameter of the inhibition zone around each sample, where bacterial growth is prevented, was measured. The size of the inhibition zone depends on the antimicrobial efficacy of the agent and its diffusion rate through the agar, which can be influenced by factors such as molecular weight and configuration. Measured zone diameters were compared with standard reference values to categorize the bacterial strain as resistant, moderately susceptible or susceptible to the tested agent.

RESULTS AND DISCUSSION

Structural studies: The XRD patterns of pure $CoFe_2O_4$, lithium-doped and nickel-doped $CoFe_2O_4$ synthesized *via* the chemical sol-gel technique are shown in Fig. 1. These results confirm the formation of a cubic spinel structure with space group $Fd\bar{3}m$, representing the successful substitution of Ni^{2+} and Li^{+} ions. The observed diffraction peaks at 2θ values of 18.64º, 30.33º, 35.63º, 37.20º, 43.21º, 53.54º, 57.20º and 62.69º correspond to the (111), (220), (311), (222), (400), (422), (511) and (440) crystallographic planes, respectively,

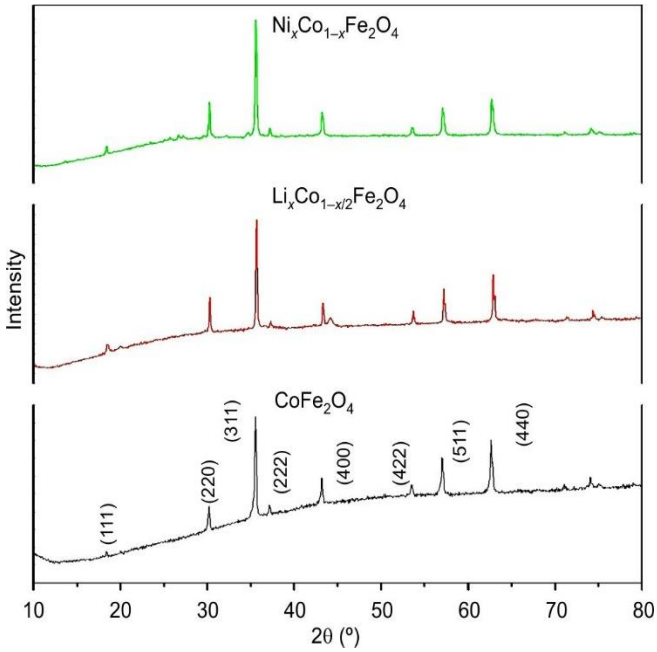

Fig. 1. (a-c) X-ray diffraction patterns of pure $CoFe_2O_4$, Li doped $CoFe_2O_4$ and Ni doped $CoFe_2O_4$ nanoparticles by sol-gel technique

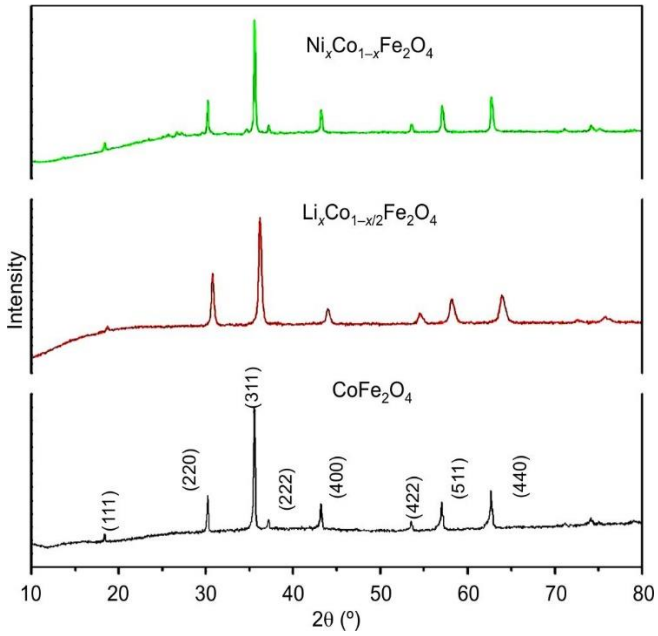

Fig. 2. (a-c) X-ray diffraction patterns of pure $CoFe_2O_4$, Li doped $CoFe_2O_4$ and Ni doped $CoFe_2O_4$ nanoparticles by green synthesis

which are characteristic of the inverse spinel structure of $CoFe_2O_4$ (JCPDS #22-1086). The absence of impurity peaks further approves purity.

Comparing the XRD patterns in Fig. 1a and c, it is observed that all peak positions remain almost same shows very small shifts in lattice parameters. A slight shift towards higher 2θ values (Fig. 1a-b) suggests a reduction in *d*-spacing in lithium doped cobalt ferrite. This indicate that lithium substitution leads to lattice contraction, improving the electrical conductivity of Li-doped cobalt ferrite in comparison to Ni-doped and pure cobalt ferrites which was further verified by Li-doped compound exhibits broader full width at half maximum (FWHM) values as shown in Table-1, suggesting a smaller crystallite size compared to Ni-doped and pure cobalt ferrites.

TABLE-1
CRYSTALLITE SIZE AND FWHM OF FERRITE SAMPLES SYNTHESIZED VIA CHEMICAL AND GREEN METHODS

Sample	Synthesis route	FWHM (°)	Crystallite size, D (nm)
$CoFe_2O_4$	Chemical	0.5077	17.8
$CoFe_2O_4$	Green	0.6125	14.7
$Ni_{0.5}Co_{0.5}Fe_2O_4$	Chemical	1.0320	8.7
$Ni_{0.5}Co_{0.5}Fe_2O_4$	Green	1.2210	7.4
$Li_{0.5}Co_{0.75}Fe_2O_4$	Chemical	0.3385	26.7
$Li_{0.5}Co_{0.75}Fe_2O_4$	Green	0.4280	21.2

The XRD patterns for green-synthesized prepared ferrite nanomaterials are shown in Fig. 2a-c. same as that of chemically synthesized compounds, the diffraction peaks correspond to a cubic spinel structure. Furthermore, the rearrangement of positions of atoms happened due to the disappearance of the (222) plane also indicates that Li^+ ions dislocate the crystallographic arrangement (Fig. 2b). Remarkably, the shifts in small peaks shifts more compared to high peaks leads to changes in the structural properties after lithium doping.

The crystallite sizes of all samples, determined using the Scherrer's equation, ranged from 20 nm to 50 nm. The lithium-doped ferrites having smaller lattice parameters compared to nickel-doped ferrites due to contraction of unit cell especially the material prepared through green synthesis method having narrower peak widths shows enhanced crystallinity.

The comparative XRD patterns of chemically and green-synthesized ferrites also reveal a noticeable shift of the main (311) diffraction peak toward higher 2θ values in the green synthesized samples, indicating a slight reduction in lattice parameter and suggesting cationic redistribution within the spinel lattice. These variations arise from the interaction of bioactive components in *A. sativum* with metal precursors, influencing crystallite growth and local strain. Hence, the green synthesis method yields highly crystalline nanoparticles with smaller crystallite sizes, making them promising candidates for biomedical and electronic applications.

Morphological studies: Scanning electron microscopy was used to study the surface morphology and particle size distribution of the prepared compounds and to compare the differences in structure with respect to method of preparation. The SEM images of both chemically and green synthesized cobalt ferrite, lithium-doped and nickel-doped cobalt ferrite, as presented in Fig. 3, indicates the uniformity and dispersion of particles. These images confirmed that $Li_{0.5}Co_{0.75}Fe_2O_4$ and $Ni_{0.5}Co_{0.5}Fe_2O_4$ exhibit relatively well distributed and homogenous nanoparticles, whereas $CoFe_2O_4$ displays more noticeable agglomeration possibly due to its stronger interparticle interactions. Heavier elements such as iron look brighter in SEM images due to their higher atomic number which improves electron scattering. This variation in particle size highlights the difference in synthesis where green technique involves in production of smaller and more stable nanoparticles with precise structural properties.

The comparison between green and chemically synthesized doped-ferrite nanoparticles also results in the distinct

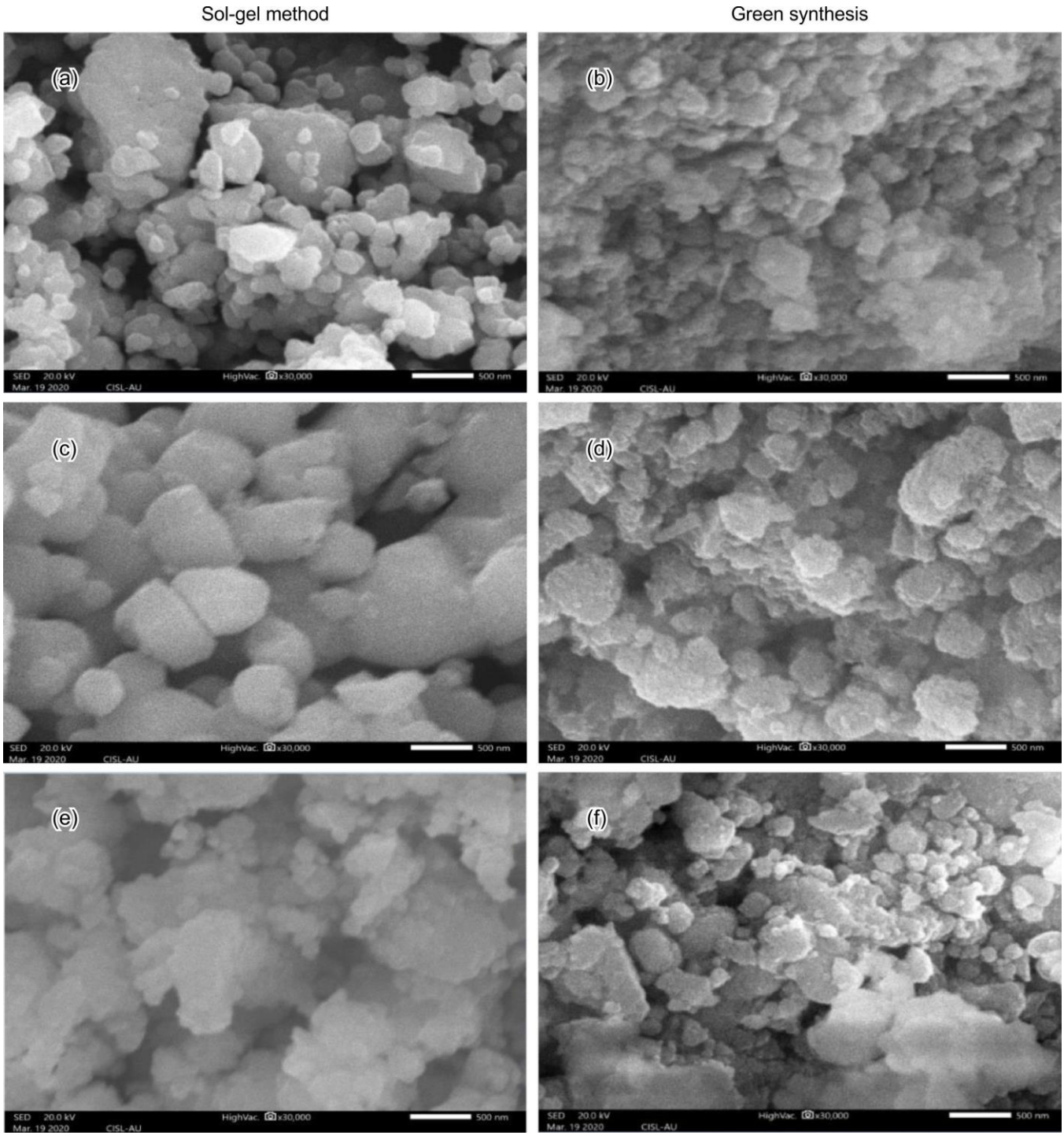

Fig. 3. SEM image of (a,b) cobalt ferrite, (c,d) Li doped cobalt ferrite and (e,f) Ni doped cobalt ferrite at 500 nm magnification

structural variations. The green synthesized doped-ferrite nanoparticles mainly showed spherical shapes whereas the chemically synthesized displayed a more cubic due to nucleation. The particle sizes of green and chemically synthesized ferrites almost match with the values from the XRD determined using Scherrer's formula [15-17].

EDS studies: The EDS analysis confirms the elemental composition further supporting the successful synthesis of $CoFe_2O_4$, $Li_{0.5}Co_{0.75}Fe_2O_4$, and $Ni_{0.5}Co_{0.5}Fe_2O_4$ with significant differences in metal ratios, oxygen content and trace element presence between sol-gel and green synthesis methods (Table-2). The comparative investigation highlights the opportunities of eco-friendly synthesis routes for synthesising high-performance ferrite nanoparticles with tailored morphology, improved stability and excellent functional properties, making them attractive candidates for catalysis, wastewater treatment and other eco-friendly applications.

FTIR studies: FTIR spectroscopy was employed to analyse the chemical properties and structure of $CoFe_2O_4$ $Ni_{0.5}Co_{0.5}Fe_2O_4$ and $Li_{0.5}Co_{0.75}Fe_2O_4$ nanoparticles, prepared

TABLE-2
EDX ELEMENTAL COMPOSITION DATA OF FERRITES PREPARED BY GREEN AND CHEMICAL METHODS

Composition	Element	Atomic (%)	
		Green	Chemical
$CoFe_2O_4$	O	52.07	53.98
	Cl	0.80	–
	K	0.68	–
	Fe	30.40	30.22
	Co	16.04	15.8
$NiCoFe_2O_4$	C	22.59	–
	O	48.96	51.3
	S	0.31	–
	Cl	0.61	–
	K	0.48	–
	Fe	18.52	35.28
	Ni	7.83	12.91
	Cu	0.70	0.51
$LiCoFe_2O_4$	O	56.09	44.65
	S	0.57	–
	K	0.49	–
	Fe	31.67	41.1
	Co	10.35	13.49
	Cu	0.83	0.76

via chemical and green methods. The FTIR spectra (Fig. 4a-c) showed the characteristic absorption bands related to both ferrite lattice vibrations and organic residues.

In green-synthesized compounds, extra absorption bands within the 3600-3300 cm^{-1} were observed, attributed to O–H stretching from surface hydroxyls and residual phytochemicals from the extract of *A. sativum*. These peaks were less intense or absent in chemically prepared ferrites, proving biological surface alteration. The C–H and C=O stretching vibrations observed in the range of 2900-2300 cm^{-1} and 1700-1600 cm^{-1} also revealed the existence of organic capping agents that stabilize nanoparticles and reduce agglomeration.

In all samples, intense metal-oxygen (M–O) stretching bands were evident near 570 cm^{-1} and 400 cm^{-1}, consistent spinel ferrites (M = Ni, Co, Li), verifying effective phase formation and cation integration into the lattice. Significantly, the chemically prepared ferrites revealed sharper and stronger M–O bands, indicating enhanced crystallinity, while green synthesized samples displayed broader peaks due to reduced grain size and surface functionalization.

In summary, the FTIR results show that green synthesis introduces biocompatible surface groups that improve nanoparticle uniformity and stability without altering the ferrite spinel structure. The observed spectral variations between green and chemical routes confirmed the dual influence of synthesis pathway and organic precursors on structural and surface chemistry.

Electrical conductivity studies: The electrical conductivity (σ) of the ferrite nanoparticles was calculated from the impedance data using the following relation:

$$\sigma = \frac{1}{\rho} = \frac{l}{R \times A}$$

where σ is conductivity (S/cm); ρ is resistivity (Ω·cm); R is bulk resistance (Ω) obtained from the low-frequency intercept of the Nyquist plot; *l* is pellet thickness; and A is electrode area.

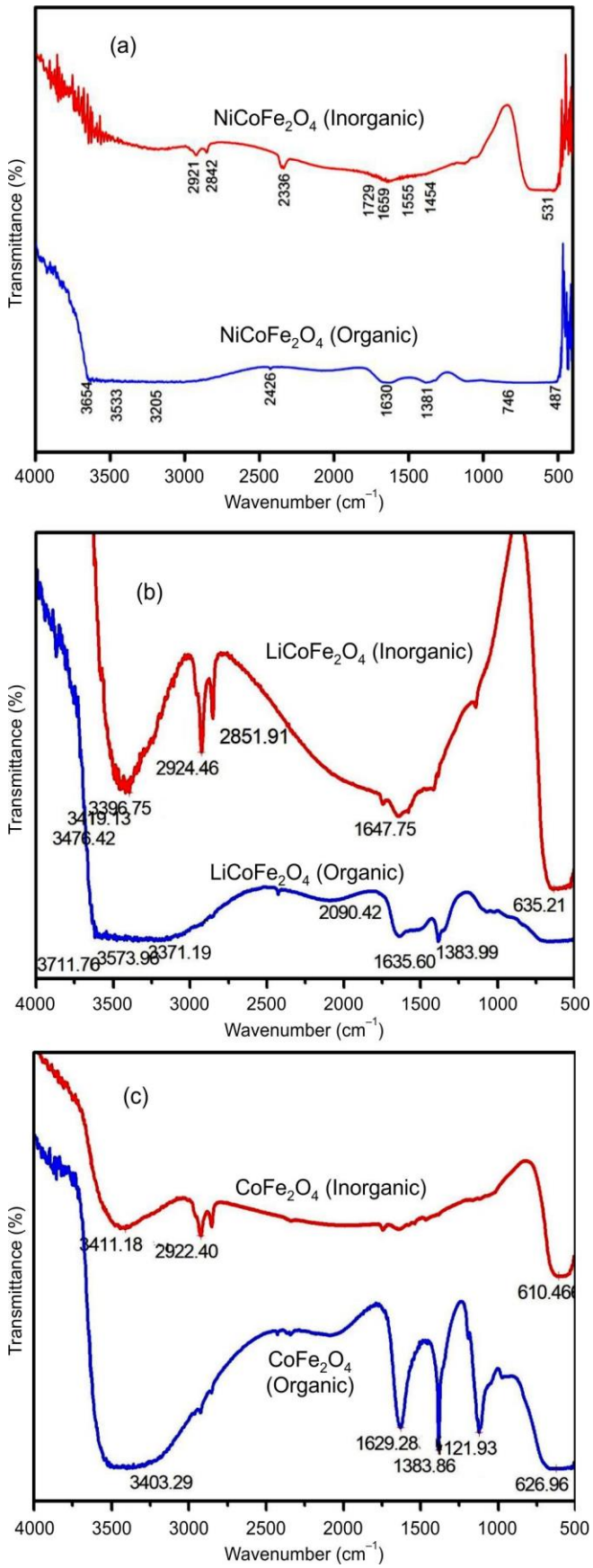

Fig. 4. IR spectra comparison of (a) $Ni_{0.5}Co_{0.5}Fe_2O_4$ (organic and inorganic), (b) $Li_{0.5}Co_{0.75}Fe_2O_4$ (organic and inorganic) and (c) $CoFe_2O_4$ (organic and inorganic)

Lower R values indicate reduced grain boundary resistance and improved charge transport (Table-3). Green synthesized samples showed lower bulk resistance and higher conductivity than chemically synthesized ones, confirming better crystallinity and enhanced electron mobility. Among all, Ni-doped ferrite (sol-gel) exhibited the highest σ, while Li-doped ferrite (green) showed excellent ionic conductivity, suitable for the lithium-ion battery anodes. Even though Ni-doped ferrite (sol-gel) showed the superior electrical conductivity (4.47×10^{-2} S cm^{-1}), mainly electronic transport limits the Li^+ mobility. Meanwhile, the green synthesized Li-doped spinel ferrite possessed balanced ionic-electronic conduction ($\sigma = 1.98 \times 10^{-3}$ S cm^{-1}), reduce polarization resistance and a porous morphology, which improves the Li^+ intercalation kinetics. These properties together make $Li_{0.5}Co_{0.75}Fe_2O_4$ (green) the most promising and sustainable candidate for use as an anode active material in LIBs.

TABLE-3
BULK RESISTANCE AND ELECTRICAL CONDUCTIVITY OF PREPARED FERRITES

Prepared compounds	Bulk resistance (Ω)	Conductivity (σ) (S/cm)
$CoFe_2O_4$ (Sol-gel method)	40.68	6.26×10^{-3}
$Li_{0.5}Co_{0.75}Fe_2O_4$ (Sol-gel method)	26.04	9.78×10^{-3}
$Ni_{0.5}Co_{0.5}Fe_2O_4$ (Sol-gel method)	5.70	4.47×10^{-2}
$CoFe_2O_4$ (Green synthesis)	160.88	1.58×10^{-3}
$Li_{0.5}Co_{0.75}Fe_2O_4$ (Green synthesis)	128.96	1.98×10^{-3}
$Ni_{0.5}Co_{0.5}Fe_2O_4$ (Green synthesis)	284.06	8.97×10^{-4}

Impedance analysis and Nyquist plot interpretation: The impedance spectra of cobalt ferrite, nickel- and lithium-doped cobalt spinal ferrites prepared *via* the green synthesis and sol-gel methods are represented as Nyquist diagrams (Cole-Cole plots) (Fig. 5). The Nyquist plots show that the green-synthesized ferrites possess reduced bulk resistance compared to chemically prepared compounds, suggesting the superior ionic conductivity. This is attributed to the reduced grain boundary resistance, enhanced particle dispersion and the bio-assisted stabilization effects provided by the green synthesis process.

Comparative conductivity and impedance analysis: The impedance spectra for $Ni_{0.5}Co_{0.5}Fe_2O_4$ as shown in Fig. 6, highlight the real (Z′) and imaginary (Z″) components of impedance *vs*. frequency. The plot highlight that the resistance (R) of green-synthesized $CoFe_2O_4$ is notably lower than its chemically fabricated counterpart, possessing enhanced conductivity. This trend is consistently observed across both Ni as well as Li-doped spinal ferrites, emphasizing the improving role of bio-assisted fabrication in enhancing charge transport characteristics.

The ionic conductivity was calculated from the inverse of resistivity, which was obtained from the low-frequency intercept of the semi-circle in the Nyquist plots. The results indicate that green-synthesized $Li_{0.5}Co_{0.75}Fe_2O_4$ exhibits the highest conductivity, making it a promising candidate for the anode materials in lithium-ion battery applications. Moreover, the impedance spectra of $CoFe_2O_4$ and $Li_{0.5}Co_{0.75}Fe_2O_4$ validating that sol-gel prepared materials exhibit more specific

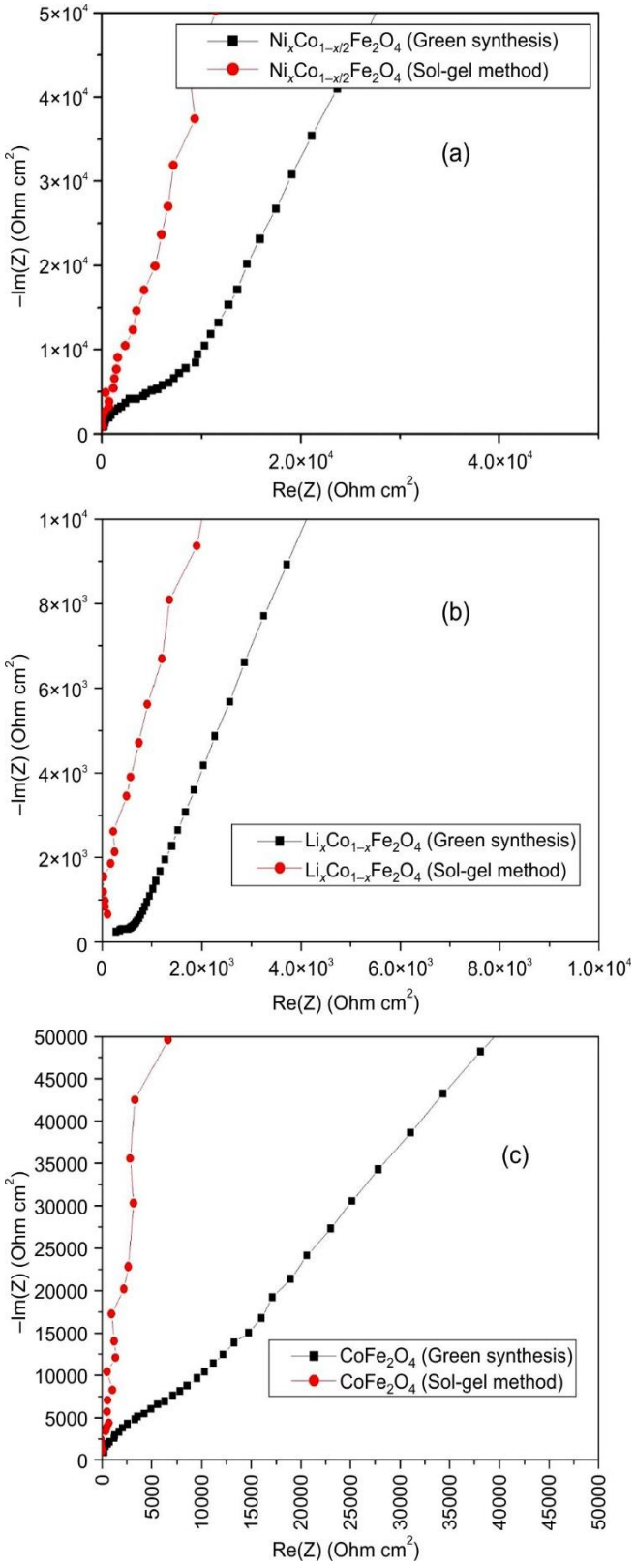

Fig. 5. Impedance spectrum for (a) $Ni_{0.5}Co_{0.5}Fe_2O_4$, (b) $Li_{0.5}Co_{0.75}Fe_2O_4$ and (c) $CoFe_2O_4$

capacity compared to their green-synthesized spinal ferrites. This variation is attributed due to thicker electrode generation in the green synthesis technique, leading to the slightly decreased charge transfer efficiency.

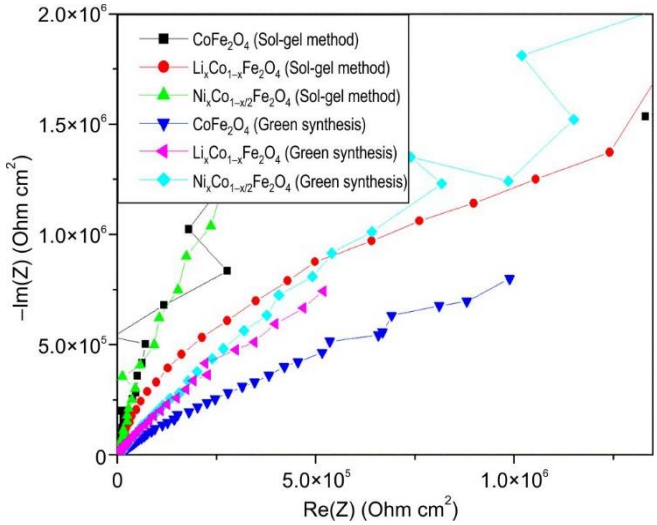

Fig. 6. Complex impedance spectra of $Ni_{0.5}Co_{0.5}Fe_2O_4$, $CoFe_2O_4$ and $Li_{0.5}Co_{0.75}Fe_2O_4$ prepared by Sol-gel technique with green and chemical agents

The unusual impedance behaviour arises from the surface organic residues and defect sites formed during the green synthesis, affect uniform charge transport and poses deviations from ideal semi-circular response. Reduced crystallite size and larger lattice strain in the green-synthesized ferrites further leads to the unusual impedance pattern. The impedance study provides compelling evidence of enhanced electrical characteristics in green-synthesized ferrites compared to chemically fabricated ones. Impedance spectroscopy showed less resistance and superior conductivity [18-21] in green synthesized compounds, particularly $Li_{0.5}Co_{0.75}Fe_2O_4$ exhibits their potential suitability as anode materials for next-generation advanced lithium-ion batteries. The enhanced electrical properties of green-synthesized ferrites result to the smaller particle size, reduced defects and better crystallinity, making them suitable for electromagnetic shielding, energy storage and spintronic applications.

Antibacterial activity: The antibacterial properties of, $CoFe_2O_4$, $Ni_{0.5}Co_{0.5}Fe_2O_4$ and $Li_{0.5}Co_{0.75}Fe_2O_4$ nanoparticles were determined by the agar well diffusion method against two clinically relevant pathogens: *Pseudomonas aeruginosa* (Gram-negative bacteria) and *Staphylococcus aureus* (Gram-positive bacteria). A comparative study between chemically and green-synthesized spinal ferrite nanoparticles implies that organic nanoparticles demonstrated enhanced antibacterial activity due to their reduced size, larger surface area and improved bioactivity. Among the fabricated ferrites, $Ni_{0.5}Co_{0.5}Fe_2O_4$ revealed the largest antibacterial effectiveness, mainly against *P. aeruginosa*, followed by $Li_{0.5}Co_{0.75}Fe_2O_4$ and $CoFe_2O_4$ (Fig. 7). These results indicate that green-synthesized ferrite nanoparticles possess significant potential as antibacterial agents for the environmental and biomedical applications.

Conclusion

This study demonstrates that both sol-gel and green synthesis routes successfully produced phase-pure $CoFe_2O_4$, $Ni_{0.5}Co_{0.5}Fe_2O_4$ and $Li_{0.5}Co_{0.75}Fe_2O_4$ ferrites with tuneable structural and functional properties. Green synthesis, aided by bioactive constituents of *Allium sativum*, yielded reduced

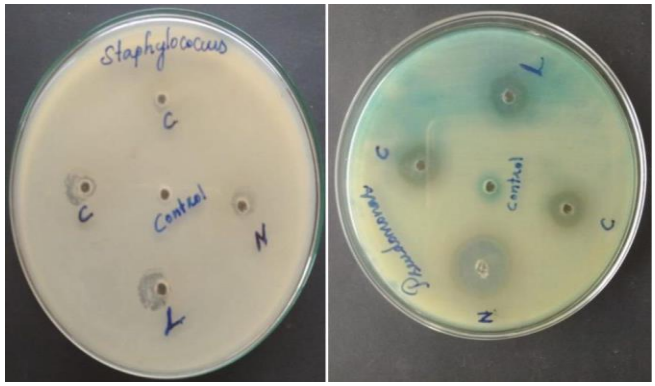

Fig. 7. Antibacterial activity of *S. aureus* and *P. aeruginosa* treated with $Ni_{0.5}Co_{0.5}Fe_2O_4$, $CoFe_2O_4$ and $Li_{0.5}Co_{0.75}Fe_2O_4$ nanoparticles

crystallites, improved the surface functionalization and lowered agglomeration, leading to enhanced ionic conductivity and increased antibacterial activity. Sol-gel compounds exhibited well-ordered crystallinity and improved electronic conductivity, mainly in Ni-doped spinal ferrite. On the whole, Li-doped ferrite prepared *via* the green route revealed promising properties for lithium-ion battery anodes, while Ni-doped spinal ferrite gave the highest antibacterial efficacy against *Pseudomonas aeruginosa*. These results highlight the potential of plant-mediated fabrication as a sustainable replacement to the chemical methods, enabling eco-friendly synthesis of multifunctional ferrites for antimicrobial coatings, energy storage and related technological applications.

CONFLICT OF INTEREST

The authors declare that there is no conflict of interests regarding the publication of this article.

REFERENCES

1. A.K. Soni and R.K. Jha, *Cureus*, **16**, e59234 (2024); https://doi.org/10.7759/cureus.59234
2. A. Baruah, R. Newar, S. Das, N. Kalita, M. Nath, P. Ghosh, H. Sarma, S. Chinnam and M. Narayan, *Discover Nano*, **19**, 103 (2024); https://doi.org/10.1186/s11671-024-04032-6
3. M. Ajaz, W. Rasool and A. Mahmood, *Futur. Biotechnol.*, **4**, 12 (2024); https://doi.org/10.54393/fbt.v4i01.81
4. M. Ramesh, R. Janani, C. Deepa and L. Rajeshkumar, *Biosensors*, **13**, 40 (2023); https://doi.org/10.3390/bios13010040
5. L. Melguizo-Rodríguez, E. García-Recio, C. Ruiz, E. De Luna-Bertos, R. Illescas-Montes and V.J. Costela-Ruiz, *Food & Function*, **13**, 2415 (2022); https://doi.org/10.1039/D1FO03180E
6. B. Yudhistira, F. Punthi, J.-A. Lin, A.S. Sulaimana, C.-K. Chang and C.-W. Hsieh, *Compr. Rev. Food Sci. Food Saf.*, **21**, 2665 (2022); https://doi.org/10.1111/1541-4337.12937
7. A. Shang, S.-Y. Cao, X.-Y. Xu, R.-Y. Gan, G.-Y. Tang, H. Corke, V. Mavumengwana and H.-B. Li, *Foods*, **8**, 246 (2019); https://doi.org/10.3390/foods8070246
8. S.J.S. Salih and W.M. Mahmood, *Heliyon*, **9**, e16601 (2023); https://doi.org/10.1016/j.heliyon.2023.e16601
9. A. Rabbani, R. Haghniaz, T. Khan, R. Khan, A. Khalid, S.S. Naz, M. Ul-Islam, F. Vajhadi and F. Wahid, *RSC Adv.*, 11, 1773 (2021); https://doi.org/10.1039/D0RA08417D
10. D.O. Morais, A. Pancotti, G.S. de Souza, M.V. Saivish, A. Braoios, M.L. Moreli, M.V. de B. Souza, V.G. da Costa and J. Wang, *J. Mater. Sci.: Mater. Med.*, **32**, 101 (2021); https://doi.org/10.1007/s10856-021-06578-8

11. M. Baričić, P. Maltoni, G. Barucca, N. Yaacoub, A. Omelyanchik, F. Canepa, R. Mathieu and D. Peddis, *Phys. Chem. Chem. Phys.*, **26**, 6325 (2024); https://doi.org/10.1039/D3CP06029B
12. B. Nawaz, G. Ali, M.O. Ullah, S. Rehman and F. Abbas, *Energies*, **14**, 3297 (2021); https://doi.org/10.3390/en14113297
13. L. Liu, Y. Li, A.A. Al-Huqail, E. Ali, T. Alkhalifah, F. Alturise and H.E. Ali, *Chemosphere*, **334**, 138638 (2023); https://doi.org/10.1016/j.chemosphere.2023.138638
14. A.A. El-Refai, G.A. Ghoniem, A.Y. El-Khateeb and M.M. Hassaan, *J. Nanostruct. Chem.*, **8**, 71 (2018); https://doi.org/10.1007/s40097-018-0255-8
15. K. Arora, L. Ledwani and Komal, *ChemistrySelect*, **10**, e202404136 (2025); https://doi.org/10.1002/slct.202404136
16. S.M. Ansari, A. Younis, Y.D. Kolekar and C. V. Ramana, *Appl. Phys. Rev.*, **12**, 021308 (2025); https://doi.org/10.1063/5.0244555
17. H. Boussafel, C. Sedrati and S. Alleg, *Appl. Phys. A*, **130**, 374 (2024); https://doi.org/10.1007/s00339-024-07547-y
18. H. Hussein, S.S. Ibrahim and S.A. Khairy, *J. Semicond.*, **46**, 122101. (2025); https://doi.org/10.1088/1674-4926/25040013
19. A.H. Bashal, M.A. Hefnawy, H.A. Ahmed, M.A. El-Atawy, R.A. Pashameah and S.S. Medany, *Nanomaterials*, **13**, 2643 (2023); https://doi.org/10.3390/nano13192643
20. H. Sultan, A. Sultan, R. Orfali, S. Perveen, T. Ali, S. Ullah, H.M. Anas, S. Ghaffar, A. Al-Taweel, M. Waqas, W. Shahzad, A. Kareem, A. Liaqat, Z. Ashraf, A. Shahid and A. Rauf, *Materials*, **15**, 5768 (2022); https://doi.org/10.3390/ma15165768
21. M. Bastianello, S. Gross, and M. T. Elm, *RSC Adv*., **9**, 33282 (2019); https://doi.org/10.1039/C9RA06310B